Phase-coherent elastic scattering of electromagnetic waves from a random array of resonant dielectric ridges on a dielectric substrate: Weak roughness limit

B. Danila and A. R. McGurn
Department of Physics, Western Michigan University, Kalamazoo, Michigan 49008, USA
(Received 29 September 2004; published 22 March 2005)

A theoretical discussion is given of the diffuse scattering of *p*-polarized electromagnetic waves from a vacuum-dielectric interface characterized by a one-dimensional disorder in the form of parallel, Gaussian shaped, dielectric ridges positioned at random on a planar semi-infinite dielectric substrate. The parameters of the surface roughness are chosen so that the surface is characterized as weakly rough with a low ridge concentration. The emphasis is on phase coherent features in the speckle pattern of light scattered from the surface. These features are determined from the intensity-intensity correlation function of the speckle pattern and are studied as functions of the frequency of light for frequencies near the dielectric frequency resonances of the ridge material. In the first part of the study, the ridges on the substrate are taken to be identical, made from either GaAs, NaF, or ZnS. The substrate for all cases is CdS. In a second set of studies, the heights and widths of the ridges are statistically distributed. The effects of these different types of randomness on the scattering from the random array of dielectric ridges is determined near the dielectric resonance frequency of the ridge material. The work presented is an extension of studies [A. B. McGurn and R. M. Fitzgerald, Phys. Rev. B **65**, 155414 (2002)] that originally treated only the differential reflection coefficient of the diffuse scattering of light (not speckle correlation functions) from a system of identical ridges. The object of the present work is to demonstrate the effects of the dielectric frequency resonances of the ridge materials on the phase coherent features found in the speckle patterns of the diffusely scattered light. The dielectric frequency resonances are shown to enhance the observation of the weak localization of electromagnetic surface waves at the random interface. The frequencies treated in this work are in the infrared. Previous weak localization studies have concentrated mainly on the visible and ultraviolet.

DOI: 10.1103/PhysRevB.71.115421 PACS number(s): 78.68.+m, 78.30.−j, 78.20.−e, 71.36.+c

I. INTRODUCTION

During the last three decades the scattering of electromagnetic waves from weak randomly rough surfaces supporting surface plasmon polaritons has been a topic of considerable interest.[1–14] In these systems surface plasmon polaritons[4] act as intermediary paths between electromagnetic waves incident on the surface and scattered waves radiating from the surface.[5–8] This increases multiple scattering processes at the random surface and enhances the overall diffuse surface scattering.[6] In turn, the participation of surface plasmon polaritons allows for the use of surface scattering to probe the nature of the surface plasmon-polaritons and the effects on them of surface disorder.[4,12] This is of particular interest in the study of weak localization phenomena arising from the interaction of surface plasmon polaritons with surface disorder.[12] Weak localization manifests itself in a number of features observed in the differential reflection coefficient and speckle correlations of light diffusely scattered from weakly rough surfaces.

The focus of the discussion in this paper is on weak localization (phase coherent multiple scattering) effects on surface plasmon polaritons and on the electromagnetic radiation elastically and diffusely scattered from weak randomly rough surfaces.[5–8] It will be shown how these effects, as observed in the speckle correlation functions for the light scattered from rough surfaces,[15–20] can be enhanced by the resonant properties (frequency resonances) of dielectric materials forming the surface.[21–24] Results will be presented for specific systems that can be experimentally realized. The discussion given complements previous work on weak localization effects in the differential reflection coefficients from such surfaces presented by us in Ref. 21.

Weak localization is observed as a backscattering enhancement in the diffuse scattering from bulk random media or in the diffuse scattering from rough surfaces,[2,5–8] arising from phase coherent multiple scattering processes represented by maximally crossed diagrams. It is a precursor of strong (Anderson) localization[5,6,8,25] which occurs when the backscattering is strong enough to confine excitations to a bounded region of space.

Since multiply scattered radiation at a random rough surface eventually radiates away from the surface, the localization observed in surface scattering is always weak localization.[6,12] The observation of true weak localization scattering enhancement peaks (as distinct from shadowing enhancement effects which are discussed below[6]), however, requires weakly rough surfaces. These are surfaces on which the length scale characterizing the roughness perpendicular to the mean surface is much less than that characterizing the roughness parallel to the mean surface and than the wavelength of the radiation. The small surface plasmon-polariton scattering cross sections generally found on such surfaces make the observation of weak localization difficult.[6] On strongly rough surfaces a backscattering enhancement can arise independently of weak localization. This is due to shadowing.[6] (Note: The total backscattering enhancement on strongly rough surfaces can be a combination of shadowing

and weak localization effects.[6] These, however, are hard to distinguish from one another.) Shadowing does not involve phase coherence but comes from the formation of patches of surface that are weakly illuminated by light (i.e., regions covered by shadows). This gives rise to backscattering enhancement features in the diffuse scattering that are similar to those due to weak localization.[6] Surfaces that allow only for the observation of weak localization in the scattered radiation must be weakly rough surfaces that scatter radiation strongly enough so that phase coherent multiple scattering processes are important. In the following some ideas proposed for the enhancement of strong localization effects in bulk three-dimensional media are used to facilitate the observation of weak localization in surface scattering.

Recently, it has been suggested in the context of strong localization[22–24] that phase-coherent cross sections in bulk three-dimensional media can be enhanced by the presence of resonant scattering features in the bulk. Waves with frequencies tuned to the resonance of the scattering features will experience an enhancement of single and, consequently, multiple scattering effects. These resonant scattering ideas, however, can also be applied to the observation of weak localization in the scattering from weakly rough surfaces.[21] Surfaces composed of resonant dielectric features should exhibit enhancement of weak localization effects near their resonant frequencies. Examples of such types of dielectric resonances that can be used are the transverse phonon Reststrahl (infrared) resonances in ionic and semiconducting materials. A previous theoretical study[21] has confirmed the phase-coherent enhancement in the differential reflection and transmission coefficients for a randomly rough surface composed of dielectric ridges exhibiting a Reststrahl resonance. The differential reflection coefficients in Ref. 21 were studied as functions of the frequency of light increasing up to the dielectric resonant frequency and the frequency of light decreasing to the dielectric resonant frequency. The present paper extends this treatment to consider weak localization effects in the speckle correlations of light scattered by rough surfaces. A variety of phase-coherent (weak localization) effects in the speckle of scattered light are enhanced by the Reststrahl resonance and are measured by statistical correlation functions (speckle correlation functions) involving averages of products of the scattered intensity of light from the surface. Ridge materials used in the studies presented here are GaAs, NaF, or ZnS. These all have well know Reststrahl resonances. This is particularly interesting as experimental studies of weak localization effects have not been made in the infrared. Following our initial studies presented in Ref. 21, the substrate treated in this paper is CdS. This substrate material supports surface plasmon polaritons at the dielectric resonant frequencies of GaAs, NaF, or ZnS ridges.

The speckle correlation function, $C(q,k|q',k')$, is the variance about its mean of the relative intensity of diffusely scattered light, $I(q|k)$.[14–20,26–31] Formally, $C(q,k|q',k') = \langle I(q|k)I(q'|k')\rangle - \langle I(q|k)\rangle\langle I(q'|k')\rangle$ where $I(q,k)$ is the incident intensity of light with wave vector component, k, parallel to the mean surface divided into the scattered light intensity with wave vector component, q, parallel to the mean surface, and the angular brackets $\langle\ \rangle$ denote an average over the surface roughness. Generally, the speckle correlation function is measured between two different sets of scattering [i.e., (q,k) and (q',k')] from the rough surface. These are separately defined for a pair of incident (i.e., k, k') and a pair of scattering directions (i.e., q, q'). The correlation function measures the statistical correlation of the bright and dark features in the diffusely scattered light arising from the two distinct scattering processes. A high degree of correlation implies an increased similarity in the intensity patterns of the two scattering processes being correlated. Phase coherent multiple scattering processes associated with the occurrence of weak localization, generally, are found to enhance the degree of correlation and hence pattern similarity between two speckle intensity patterns.[14–20,24,26–31]

While the diffuse scattering cross section is proportional to the two-particle surface plasmon-polariton Green's function, the speckle correlation function is related to a four-particle surface plasmon-polariton Green's function.[14–20,24,26–31] The four-particle Green's function is formed from the product of the pair of two-particle Green's functions describing the two different diffuse scattering processes being correlated. It has been shown[18,19,26–31] that the speckle correlation function is a sum of successively higher order contributions in a perturbation expansion in terms of the surface roughness. The contributions to $C(q,k|q',k')$ are denoted $C^{(1)}(q,k|q',k')$, $C^{(10)}(q,k|q',k')$, $C^{(1.5)}(q,k|q',k')$, $C^{(2)}(q,k|q',k')$, and $C^{(3)}(q,k|q',k')$ so that $C=C^{(1)}+C^{(10)}+C^{(1.5)}+C^{(2)}+C^{(3)}$.[18,19] The most prominent of these contributions are the $C^{(1)}$ (see Ref. 20) and $C^{(10)}$ (see Ref. 19) short range correlations. These both occur in the lowest order of the perturbation expansion. The $C^{(1)}$ term contains the important phase coherent effects, known as the memory and time-reversed memory peaks.[18,19,27–29,31] The presence of the memory peak (i.e., a peak at $k=k'$) results from the high degree of correlation in the speckle intensities that arises from light traveling on nearly identical scattering paths. The time-reversed memory peak (i.e., a peak at $q=-k'$) accounts for the high correlation that exists between light traveling on a given scattering path and light traveling in a time-reversed manner along the same path. Other contributions are the medium and long range correlations denoted by $C^{(1.5)}$ and $C^{(2)}$,[14,18,19,26–31] respectively. These higher order terms contain peaks arising from geometric effects in momentum space and from the poles of the surface plasmon-polariton single particle Green's functions, not from phase-coherent processes. Finally, the infinite range term $C^{(3)}$ is a smoothly varying function of the incident and scattering directions. The primary interest in this paper is in the short range $C^{(1)}$ and $C^{(10)}$ contributions. These are the dominant features of the speckle correlation function and contain the phase-coherent effects. For completeness and comparison results for $C^{(1.5)}$, $C^{(2)}$, and $C^{(3)}$ are also given.

The model considered in the first set of studies presented in this paper involves a surface exhibiting one-dimensional disorder in the form of parallel, Gaussian shaped, dielectric ridges positioned at random on a planar semi-infinite dielectric substrate surface.[21] The number of ridges per unit length of the interface is chosen to be small enough that there is only a small possibility of overlapping between the ridges. The ridges are identical and made from either GaAs, NaF, or ZnS, while the substrate material is always CdS. The differ-

ential reflection and transmission coefficients of the diffuse scattering for these systems were presented in Ref. 21. In this paper the contributions to the speckle correlation functions for the diffuse scattering computed as functions of the ridge concentration are presented.

In a second set of studies, the ridges are no longer taken to be identical. In addition to their positions on the surface, the ridge widths and heights are statistically distributed. The sensitivity of the speckle correlation function to parameters characterizing this statistical distribution is determined. The shape of the peaks in the correlation function is related to the average and the standard deviation of the width and height distributions. In addition, for these types of systems (not treated in Ref. 21) a study is presented of the effects of the statistical distribution of ridge properties on the differential reflection coefficients. The widths and heights of the enhanced backscattering peaks are related to the average and standard deviation of the width and height distributions for the ridges.

The calculation of the correlation functions and differential reflection coefficients of the diffuse scattering is done using diagrammatic techniques.[6,12,18,19,21] Maxwell equations are solved for a single ridge to leading order in terms of its height and width, obtaining the electromagnetic scattering potential of the ridge. This potential is generalized to describe the scattering from a surface with a low concentration of randomly placed ridges. Using this, the speckle correlation functions and differential reflection coefficients are expressed in terms of ladder and maximally crossed diagrams, giving the multiple scattering contribution from the random array of ridges at the surface. These are used to compute both the two and four-particle Green's functions. For the case in which the ridge widths and heights are statistically distributed, the diffuse scattering and the speckle correlation function are averaged over both the ensemble of realizations of the array of ridges along the surface and the statistical properties of the individual ridge widths and heights.

II. MODEL AND SPECKLE CORRELATION FUNCTION: IDENTICAL SET OF RIDGES

In this section, a brief description of the rough surface is given. This is followed by a treatment of the speckle correlation functions for the diffusely scattered light from the surface. The model of the scattering surface is that used in Ref. 21 to discuss resonance effects on the differential reflection coefficient.

The random surface consists of an array of parallel Gaussian cylinder shaped dielectric ridges of dielectric constant ϵ_1 that are randomly placed on a semi-infinite substrate of dielectric constant ϵ_0. The surface of the substrate is located at the $x_3=0$ plane with the substrate in the region $x_3<0$. On the substrate is the array of Gaussian ridges and above the random surface formed by the array of Gaussian ridges is vacuum. The x_3 axis is perpendicular to the substrate surface, the x_2 axis is parallel to the axes of the ridges, and the x_1-x_3 plane is the scattering plane. The average number of ridges per unit length on the x_1 axis is such that the likelihood of a strong overlap between two ridges is small, and the positions of the ridges on the substrate surface are uncorrelated. The surface profile function $x_3=\zeta(x_1)$ of the upper surface of the Gaussian ridges is

$$\zeta(x_1) = A\sum_j e^{-((x_1 - x_{1j})/R)^2}, \tag{1}$$

where A, R, and x_{1j} are parameters characterizing the height, width, and center position of the jth ridge.

For the results presented below the substrate material is CdS while the ridge material is either GaAs, NaF, or ZnS. All of these materials exhibit a characteristic Reststrahl resonance at their transverse phonon frequencies. The general form of the dielectric constant in the neighborhood of this resonance is

$$\epsilon(\omega) = \epsilon_\infty \frac{\omega_L^2 - \omega^2 - i\dfrac{\omega}{\tau}}{\omega_T^2 - \omega^2 - i\dfrac{\omega}{\tau}}, \tag{2}$$

where ϵ_∞, ω_L, ω_T, and τ are constants characterizing the material. (The reader is referred to Ref. 21 for the values of these constants.) The ridge materials have been chosen to have dielectric resonances at frequencies for which CdS has a dielectric constant less than -1. Under these conditions surface plasmon polaritons exist on the CdS-vacuum interface.

The surface plasmon polaritons are scattered on the interface by the randomly positioned ridges. This surface scattering is enhanced for surface plasmon polaritons with frequencies near the dielectric resonance of the ridge materials. This increases the importance of phase-coherent multiple scattering effects at the surface. In addition, near the dielectric resonance frequency, the coupling between the surface plasmon polaritons and bulk electromagnetic modes above and below the surface is increased.

In our scattering geometry, the surface is illuminated by a p-polarized electromagnetic plane wave incident from vacuum. The scattering amplitude is obtained by applying electromagnetic boundary conditions to the solutions of the Maxwell equations above the surface, inside the ridges, and in the substrate material. In doing this the validity of the Rayleigh hypothesis is assumed.[6,12,21] The general form of the x_2 component of the magnetic field is[21]

$$H_2^{vac}(x_1,x_3) = e^{ikx_1 - i\alpha_0(k,\omega)x_3} + \int \frac{dq}{2\pi} R(q|k) e^{iqx_1 + i\alpha_0(q,\omega)x_3} \tag{3}$$

for $x_3 > \zeta(x_1)$,

$$H_2^{rid}(x_1,x_3) = \int \frac{dq}{2\pi} [A(q|k)e^{iqx_1 + i\alpha_1(q,\omega)x_3} + B(q|k)e^{iqx_1 - i\alpha_1(q,\omega)x_3}] \tag{4}$$

for $0 < x_3 \leqslant \zeta(x_1)$, and

$$H_2^{sub}(x_1,x_3) = \int \frac{dq}{2\pi} S(q|k) e^{iqx_1 - i\alpha(q,\omega)x_3} \tag{5}$$

for $x_3 \leqslant 0$. Following Ref. 21, the horizontal components of the incident and scattered wave vectors are denoted by k and q, respectively, and the vertical wave vector components in the three regions are $\alpha_0(p,\omega) = \sqrt{(\omega/c)^2 - p^2}$, $\alpha_1(p,\omega) = \sqrt{\epsilon_1(\omega)(\omega/c)^2 - p^2}$, and $\alpha(p,\omega) = \sqrt{\epsilon_0(\omega)(\omega/c)^2 - p^2}$. In Eqs. (3)–(5) the real and imaginary parts of α_0, α_1, and α are positive.

By matching boundary conditions, the scattering amplitude $R(q|k)$ is found to be of the form[21]

$$R(q|k) = 2\pi\delta(q-k)R_0(k,\omega) - 2iG_0(q,\omega) \times T(q|k)G_0(k,\omega)\alpha_0(k,\omega). \tag{6}$$

In Eq. (6)

$$R_0(k,\omega) = \frac{\epsilon_0(\omega)\alpha_0(k,\omega) - \alpha(k,\omega)}{\epsilon_0(\omega)\alpha_0(k,\omega) + \alpha(k,\omega)} \tag{7}$$

is the Fresnel coefficient for the reflection of p-polarized light at a flat dielectric surface, and

$$G_0(k,\omega) = \frac{i\epsilon_0}{\epsilon_0\alpha_0(k,\omega) + \alpha(k,\omega)} \tag{8}$$

is the single-particle surface plasmon-polariton Green's function for a flat surface. The scattering matrix $T(q|k)$ is a solution of[4–8]

$$T(q|k) = V(q|k) + \int \frac{dp}{2\pi} V(q|p)G_0(p)T(p|k), \tag{9}$$

where $V(q|k)$ is the scattering potential, given to leading order in the Fourier transform of the surface profile function, $\hat{\zeta}(p) = \int dx_1 \zeta(x_1)\exp(-ipx_1)$, by

$$V(q|k) \approx \frac{\epsilon_1 - 1}{\epsilon_1\epsilon_0^2}[\epsilon_0^2 qk - \epsilon_1\alpha(q)\alpha(k)]\hat{\zeta}(q-k). \tag{10}$$

A useful function to consider in our formulation is the Green's function, $G(q|k)$, for surface plasmon polaritons on the random interface. It is defined in terms of the **T** matrix of Eq. (9) by[21]

$$G(q|k) = 2\pi\delta(q-k)G_0(k) + G_0(q)T(q|k)G_0(k) \tag{11}$$

and can be studied by standard diagrammatic techniques. In addition, using Eqs. (6) and (11) both the differential reflection coefficients and speckle correlation functions can be written in terms of $G(q|k)$.

The scattering efficiency, $I(q|k)$, is defined as the ratio of the x_3 component of the outgoing Poynting vector to the x_3 component of the incoming Poynting vector[5,12,21] above the randomly rough interface. For the diffuse scattering from the rough interface

$$I(q|k) = \frac{1}{2\pi L}\frac{\alpha_0(q)}{\alpha_0(k)}|R(q|k)|^2 = \frac{2}{\pi L}\alpha_0(q)\alpha_0(k)|G(q|k)|^2, \tag{12}$$

where L is the length in the x_1 direction of the surface. The differential reflection coefficient, $dR_e/d\theta_s$, is obtained by averaging the scattering efficiency over the rough interface so that[21]

$$\frac{dR_e}{d\theta_s}(q|k) = \langle I(q|k)\rangle\frac{dq}{d\theta_s} = \frac{2}{\pi L}\alpha_0^2(q)\alpha_0(k)\langle|G(q|k)|^2\rangle. \tag{13}$$

The two-particle Green's function, $\langle|G(q|k)|^2\rangle$, containing the physics in Eq. (13) is obtained as the solution of a Bethe-Salpeter equation that is discussed below.

The speckle correlation function, $C(q,k|q',k')$, is defined[18,19] as

$$C(q,k|q',k') = \langle I(q|k)I(q'|k')\rangle - \langle I(q|k)\rangle\langle I(q'|k')\rangle \tag{14}$$

so that from Eqs. (6), (11), (12), and (14):

$$C(q,k|q',k') = \left(\frac{2}{\pi L}\right)^2 \alpha_0(q)\alpha_0(k)\alpha_0(q')\alpha_0(k') \times [\langle|G(q|k)|^2|G(q'|k')|^2\rangle - \langle|G(q|k)|^2\rangle\langle|G(q'|k')|^2\rangle] \tag{15}$$

for diffuse scattering. Making the factorization approximation[18–20]

$$\langle|G(q|k)|^2|G(q'|k')|^2\rangle \approx \langle|G(q|k)|^2\rangle\langle|G(q'|k')|^2\rangle + \langle G^*(q|k)G(q'|k')\rangle \times\langle G(q|k)G^*(q'|k')\rangle + \langle G^*(q|k)G^*(q'|k')\rangle \times\langle G(q|k)G(q'|k')\rangle, \tag{16}$$

$$C(q,k|q',k') = F(q,k|q',k')[\langle G^*(q|k)G(q'|k')\rangle \times\langle G(q|k)G^*(q'|k')\rangle + \langle G^*(q|k)G^*(q'|k')\rangle \times\langle G(q|k)G(q'|k')\rangle], \tag{17}$$

where

$$F(q,k|q',k') = \left(\frac{2}{\pi L}\right)^2 \alpha_0(q)\alpha_0(k)\alpha_0(q')\alpha_0(k'). \tag{18}$$

[Note: Equation (16) is sufficient to treat the dominant features of the diffuse scattering in our model, and the phase coherent properties of the speckle correlation function for weakly rough surfaces are reasonably well given. Section V gives addition discussion of these points.] We now turn to a discussion of the two-particle Green's functions occurring in Eqs. (13) and (17).

The averages on the right-hand sides of Eqs. (13), (16), and (17) are solutions of the Bethe-Salpeter equations[5,12,18,19,21]

$$\langle G^*(q|k)G(q'|k')\rangle = 2\pi\delta(q-k)G^*(k)2\pi\delta(q'-k')G(k') + G^*(q)G(q') \times \int \frac{dr}{2\pi}\int \frac{ds}{2\pi}\langle\Gamma(q,r|q',s)\rangle \times\langle G^*(r|k)G(s|k')\rangle, \tag{19}$$

$$\langle G(q|k)G(q'|k')\rangle = 2\pi\delta(q-k)G(k)2\pi\delta(q'-k')G(k') + G(q)G(q')\int \frac{dr}{2\pi}\int \frac{ds}{2\pi}\langle\widetilde{\Gamma}(q,r|q',s)\rangle \times\langle G(r|k)G(s|k')\rangle. \tag{20}$$

Here $\langle G(q|k)\rangle = 2\pi\delta(q-k)G(k)$ while $\langle\Gamma(q,r|p,s)\rangle$ and $\langle\widetilde{\Gamma}(q,r|p,s)\rangle$ are appropriate irreducible four vertex functions. To the lowest order in $\hat{\zeta}$[4–7]

$$\langle\Gamma(q,r|p,s)\rangle \approx \langle V^*(q|r)V(p|s)\rangle - \langle V^*(q|r)\rangle\langle V(p|s)\rangle,$$

$$\langle\widetilde{\Gamma}(q,r|p,s)\rangle \approx \langle V(q|r)V(p|s)\rangle - \langle V(q|r)\rangle\langle V(p|s)\rangle. \tag{21}$$

so that Eq. (10) gives

$$\langle\Gamma(q,r|p,s)\rangle \approx v^*(q|r)v(p|s)[\langle\hat{\zeta}^*(q-r)\hat{\zeta}(p-s)\rangle - \langle\hat{\zeta}^*(q-r)\rangle\langle\hat{\zeta}(p-s)\rangle],$$

$$\langle\widetilde{\Gamma}(q,r|p,s)\rangle \approx v(q|r)v(p|s)[\langle\hat{\zeta}(q-r)\hat{\zeta}(p-s)\rangle - \langle\hat{\zeta}(q-r)\rangle\langle\hat{\zeta}(p-s)\rangle], \tag{22}$$

where

$$v(q|k) = \frac{\epsilon_1 - 1}{\epsilon_1\epsilon_0^2}[\epsilon_0^2 qk - \epsilon_1\alpha(q)\alpha(k)]. \tag{23}$$

To compute the irreducible four vertex functions in Eqs. (21) and (22), the Fourier transform of the surface profile function is needed. This is obtained[21] by discretizing the x_1 axis and taking the Gaussian ridges to be centered at the vertices of the one-dimensional lattice given by $x_{1n}=n\Delta x$ for n running over the integers. For this discretization $\Delta x \ll R$. Denoting c_n as the occupation index of vertex n, $c_n=1$ if a ridge is centered at $n\Delta x$ and $c_n=0$ otherwise. Upon averaging over the surface $\langle c_n\rangle=\langle c_n^2\rangle=c_{av}$, and the average number of ridges per unit length is $N=c_{av}/\Delta x$. The Fourier transform of the profile function is

$$\hat{\zeta}(p) = \sqrt{\pi}ARe^{-p^2R^2/4}\sum_n c_n e^{-inp\Delta x}. \tag{24}$$

From Eqs. (22)–(24) the average irreducible four vertex function $\langle\Gamma\rangle$ to lowest order becomes

$$\langle\Gamma(q,r|p,s)\rangle = 2\pi\delta(q-r-p+s)\Gamma_0(q,r|p,s) \tag{25}$$

with

$$\Gamma_0(q,r|p,s) \approx \frac{\pi}{\Delta x}(c_{av}-c_{av}^2)v^*(q|r)v(p|s)A^2R^2e^{-(q-r)^2(R^2/2)}. \tag{26}$$

Similarly $\langle\widetilde{\Gamma}\rangle$ to lowest order becomes

$$\langle\widetilde{\Gamma}(q,r|p,s)\rangle = 2\pi\delta(q-r+p-s)\widetilde{\Gamma}_0(q,r|p,s) \tag{27}$$

with

$$\widetilde{\Gamma}_0(q,r|p,s) \approx \frac{\pi}{\Delta x}(c_{av}-c_{av}^2)v(q|r)v(p|s)A^2R^2e^{-(q-r)^2(R^2/2)}. \tag{28}$$

For a discussion of weak localization effects in the speckle correlation functions the lowest order four vertex function in Eqs. (25) and (26) must be modified to include additional higher order terms in the scattering potential. These are needed to obtain a more complete set of phase coherent scattering processes, responsible for the so-called time-reversed memory effects. In addition to the lowest order term in $\langle\Gamma(q,r|p,s)\rangle$ in Eq. (26) it is necessary to include at least the lowest maximally crossed diagrammatic contribution to the irreducible four vertex. This is given by

$$\Gamma_0^{add}(q,r|p,s) = \int \frac{du}{2\pi}\Gamma_0(q,q+s-u|u,s)G^*(q+s-u)G(u)\Gamma_0(q+s-u,r|p,u). \tag{29}$$

With the inclusion of the process in Eq. (29), $\langle\Gamma(q,r|p,s)\rangle$ becomes

$$\langle\Gamma(q,r|p,s)\rangle \approx 2\pi\delta(q-r-p+s)[\Gamma_0(q,r|p,s) + \Gamma_0^{add}(q,r|p,s)]. \tag{30}$$

(Note: A similar set of maximally crossed contributions to the irreducible four vertex $\langle\widetilde{\Gamma}(q,r|p,s)\rangle$ does not lead to interesting phase coherent effects and is not treated here.) For the discussion of weak localization presented below, the irreducible four vertex function $\langle\Gamma\rangle$ is given by Eqs. (25) and (30) and the irreducible four vertex function $\langle\widetilde{\Gamma}\rangle$ is given by Eqs. (27) and (28).

The average single-particle Green's function $G(k)$ in Eqs. (19), (20), and (29) is given by[5,12,18,19,21]

$$G(k) = \frac{1}{G_0^{-1}(k)-\Sigma(k)}, \tag{31}$$

where $\Sigma(k)$ is the self-energy correction. We compute $\Sigma(k)$, in the coherent potential approximation,[5,12,18,19,21] as the solution of the self-consistent integral equation

$$\Sigma(k) = V_0(k) + \int \frac{dp}{2\pi}\frac{\widetilde{\Gamma}_0(p,k|p,k)}{G_0^{-1}(p)-\Sigma(p)} \tag{32}$$

where $V_0(k)=\sqrt{\pi}c_{av}AR/\Delta x v(k|k)$. Equation (32) is solved by iteration, using $\Sigma(k)\approx V_0(k)$ as the lowest order approximation.

III. RESULTS FOR IDENTICAL RIDGES

The Bethe-Salpeter Eqs. (19) and (20) are solved using the method in Refs. 5, 12, 18, 19, and 21. For $C^{(1)}$, however, we retain only contributions of the first two ladder diagrams and the lowest maximally crossed diagram and for $C^{(10)}$ only the lowest order ladder diagram. In terms of the surface roughness, $C^{(1)}$ and $C^{(10)}$ are both of order $\zeta^4 L^2$. The speckle correlation function within this approximation is written as[18,19]

$$C(q,k|q',k') \approx C^{(1)}(q,k|q',k') + C^{(10)}(q,k|q',k'), \quad (33)$$

where

$$C^{(1)}(q,k|q',k') = 2\pi L\,\delta(q-k-q'+k')C_0^{(1)}(q,k|q',k'), \quad (34)$$

$$C^{(10)}(q,k|q',k') = 2\pi L\,\delta(q-k+q'-k')C_0^{(10)}(q,k|q',k'), \quad (35)$$

with envelop functions

$$C_0^{(1)}(q,k|q',k') = H(q,k|q',k')|\hat{L}(q,k|q',k')|^2, \quad (36)$$

$$C_0^{(10)}(q,k|q',k') = H(q,k|q',k')|\tilde{\Gamma}_0(q,k|q',k')|^2. \quad (37)$$

In Eqs. (36) and (37)

$$H(q,k|q',k') = F(q,k|q',k')|G(q)G(k)G(q')G(k')|^2, \quad (38)$$

where

$$F(q,k|q',k') = (2/\pi L)^2(\omega/c)^4 \cos\theta_s \cos\theta_i \cos\theta_s' \cos\theta_i'.$$

In Eq. (36) $\hat{L}$ is given by[18,19]

$$\begin{aligned}\hat{L}(q,k|q',k') = \Gamma_0(q,k|q',k') &+ \int \frac{ds}{2\pi}\Gamma_0(q,q-q'+s|q',s) \\ &\times G^*(q-q'+s)G(s)\Gamma_0(q-q'+s,k|s,k') \\ &+ \int \frac{ds}{2\pi}\Gamma_0(q,q+k'-s|s,k')G^*(q+k' \\ &- s)G(s)\Gamma_0(q+k'-s,k|q',s), \end{aligned} \quad (39)$$

where $\Gamma_0(q,r|p,s)$ is defined in Eq. (26). The first and second terms on the right hand side of Eq. (39) are the first two ladder diagram contributions to the reducible four vertex of the $\langle G^*G\rangle$ two-particle Green's function. The memory effect arises from the ladder diagram of the second term. The third term on the right hand side of Eq. (39) is the maximally crossed contribution to the $\langle\Gamma\rangle$ irreducible four vertex. This was discussed in Eqs. (29) and (30) and is responsible for the time-reversed memory effects.

From Eqs. (34) and (35) it is seen that the $C^{(1)}$ and $C^{(10)}$ contributions to the correlation function are non zero only for $q-k-q'+k'=0$ and $q-k+q'-k'=0$, respectively. These conditions on q, q', k, k' are satisfied in the plots of the envelop functions $C_0^{(1)}(q,k|q',k')$ and $C_0^{(10)}(q,k|q',k')$ presented below. To facilitate the discussions, the horizontal components of the wavevectors (q, k, q', and k') are written in terms of the angles of incidence (θ_i,θ_i') and scattering (θ_s,θ_s') where

$$k = \frac{\omega}{c}\sin\theta_i, \quad q = \frac{\omega}{c}\sin\theta_s,$$

$$k' = \frac{\omega}{c}\sin\theta_i', \quad q' = \frac{\omega}{c}\sin\theta_s'. \quad (40)$$

The components of the speckle correlation function are then given in terms of the angle variables in Eq. (40). Due to the constraints on the sets of incident and scattered wave vectors, fixing two angles (i.e., θ_i and θ_s) allows us to study the nonzero envelope functions $C_0^{(1)}(q,k|q',k')$ (for which $q-k-q'+k'=0$) and $C_0^{(10)}(q,k|q',k')$ (for which $q-k+q'-k'=0$) as functions of a third angle (i.e., θ_s'). For a comparison of the speckle correlation functions with the differential reflection coefficients in Ref. 21, the parameters characterizing the rough surface are taken to be the same as those in Ref. 21. Specifically, the interface is characterized by $(\omega_T^{ridge}/c)\Delta x=0.1$, $(\omega_T^{ridge}/c)A=0.05$, $(\omega_T^{ridge}/c)R=1.0$, and the average occupancy number $c_{av}=0.001$.

Plots of $C_0^{(1)}(q,k|q',k')$ and $C_0^{(10)}(q,k|q',k')$ for rough surface geometries formed from GaAs, NaF, or ZnS on a CdS substrate are presented, respectively, in Figs. 1 and 2 for a selection of frequencies of light in the neighborhood of the resonance frequency of the dielectric material of the ridges. For these plots we have taken $\theta_i=20°$ and $\theta_s=-10°$ fixed, allowing θ_s' to run from $-90°$ to $90°$. (This angular parameterization facilitates comparison with results published on other systems.[18,19]) The $C^{(1)}$ and $C^{(10)}$ terms are the two largest contributions to the speckle correlation function and are both of the same magnitude for a given frequency of light. Of the two, only $C_0^{(1)}(q,k|q',k')$ contains weak localization effects. These are found as two peaks in the angular plot of $C^{(1)}$ occurring at $\theta_s'=-10°$ and $\theta_s'=-20°$. These peaks are known, respectively, as the memory effect and time-reversed memory effect peaks and are clearly seen in the systems of GaAs and NaF ridges. For the system of ZnS ridges the two peaks overlap to form one as the dielectric resonance frequency is approached from below. Above the dielectric resonance frequency the ZnS ridges exhibit a single peak formed from the overlap of the memory and time-reversed memory peaks. In the plots presented in Figs. 1 and 2 curves are shown for different frequencies approaching the resonant frequency (i.e., $\omega=\omega_T$ of the ridge material) both from above and below. The areas under the curves are each normalized to unity so that, for curves generated at different frequencies, the relative importance of features associated with weak localization can be compared to the general diffuse correlations. The localization effects are seen to be enhanced as the resonant frequency is approached, being significant only in the immediate neighborhood of the resonant frequency of the ridge material. The frequency intervals, centered about the resonant frequency, over which the weak localization peaks in $C^{(1)}$ are observable are similar to those for the weak localization peaks in the differential reflection coefficients ob-

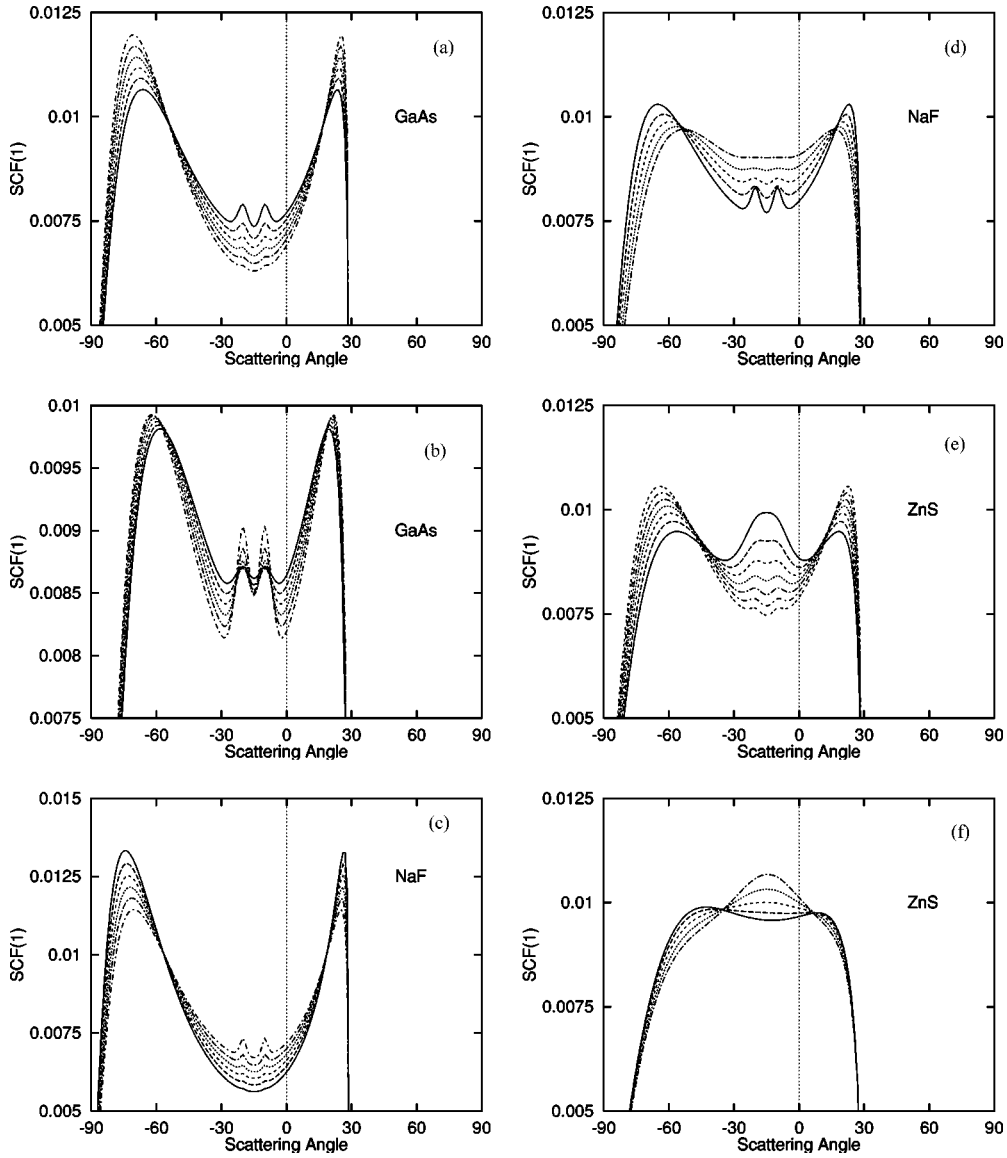

FIG. 1. Plot of $C^{(1)}(q,k|q',k')$ vs θ_s' for $\theta_i=20°$ and $\theta_s=-10°$. Results are shown for (a) GaAs for $\omega/\omega_T^{GaAs}=0.968$, 0.972, 0.976, 0.980, 0.984, 0.988 (bottom to top between scattering angles of −30° and 0°); (b) GaAs for $\omega/\omega_T^{GaAs}=1.010$, 1.012, 1.014, 1.016, 1.018, 1.020 (top to bottom at the two localization peaks); (c) NaF for $\omega/\omega_T^{NaF}=0.968$, 0.972, 0.976, 0.980, 0.984, 0.988 (bottom to top between scattering angles of −30° and 0°); (d) NaF for $\omega/\omega_T^{NaF}=1.02$, 1.03, 1.04, 1.05, 1.06 (bottom to top at the two localization peaks); (e) ZnS for $\omega/\omega_T^{ZnS}=0.956$, 0.960, 0.964, 0.968, 0.972, 0.976, 0.980 (bottom to top between scattering angles of −30° and 0°); (f) ZnS for $\omega/\omega_T^{ZnS}=1.020$, 1.018, 1.016, 1.014, 1.012 (bottom to top between −30° and 0°). All curves have been normalized to have unit area under the curve, and $C^{(1)}(q,k|q',k')$ is non-zero for $-90° \leqslant \theta_s' \leqslant 28.97°$. The resonance frequency is $\omega/\omega_T^{ridge}=1.0$.

served in Ref. 21. Consequently, Fig. 1 indicates the usefulness of the dielectric resonance for the observation of weak localization in speckle correlations in addition to the general diffuse scattering cross sections. There are no weak localization features in $C_0^{(10)}(q,k|q',k')$, and Fig. 2 is presented for completeness and comparison with $C_0^{(1)}(q,k|q',k')$.

Each of the three ridge materials treated in Fig. 1 is characterized by a range of frequencies over which the weak localization effects (memory effect from the second ladder term and time-reversed memory effect from the maximally crossed term) are significant compared to those of the slowly varying background (first ladder term) contribution. To quantify this range, the ratio of the amplitudes of the phase-coherent peaks to the background contribution as a function of frequency is estimated. Specifically, the absolute value of the ratio of the contributions to $L(q,k|q',k')$ from the first ladder diagram divided into the sum of the contributions of the second ladder and first maximally crossed diagrams at $\theta_s'=-10°$ for the memory effect peak and at $\theta_s'=-20°$ for the time-reversed memory effect peak is studied. This gives a reasonable indication of the relative importance of the phase coherent and non phase coherent contributions to $C^{(1)}\times(q,k|q',k')$. Results of this ratio for the memory effect and time-reversed memory effect are presented in Fig. 3 as functions of ω/ω_T^{ridge}. (Note: The results in Fig. 3 for the memory effect and time-reversed memory effect cannot be distin-

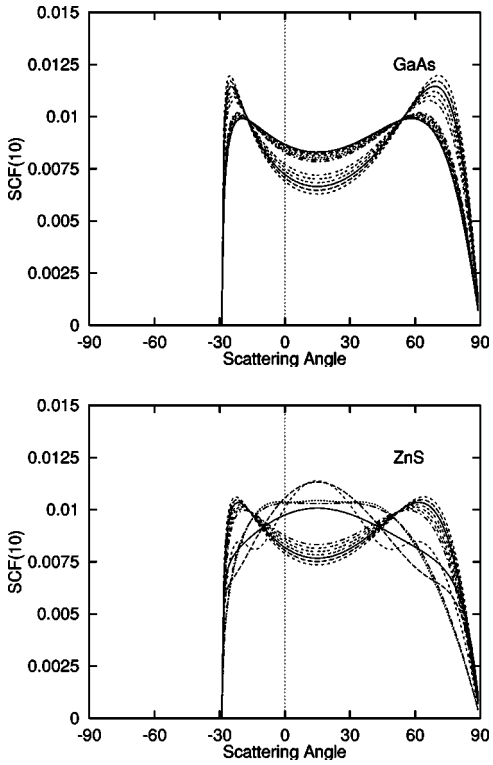

FIG. 2. Plot of $C^{(10)}(q,k|q',k')$ vs θ_s' for $\theta_i=20°$ and $\theta_s=-10°$. Results are presented for (a) GaAs at the frequencies in Fig. 1(a) (lower bundle of six curves between scattering angles of 0° and 30°) and in Fig. 1(b) (upper bundle of six curves between scattering angles of 0° and 30°) and (b) ZnS at the frequencies in Fig. 1(e) (lower bundle of seven curves between scattering angles of 0° and 30°) and the remaining five curves are at the frequencies of Fig. 1(f). The ordering within each bundle is the same as in Fig. 1. All curves have been normalized to have unit area under the curve, and $C^{(10)}(q,k|q',k')$ is non-zero for $-28.97° \leqslant \theta_s' \leqslant 90°$. Note: A similar relationship between $C^{(1)}$ and $C^{(10)}$ to those found for GaAs and ZnS exists for NaF, but for brevity plots of $C^{(10)}$ for NaF have been omitted here.

guished on the scale of the figure.) Curves are shown for each of the ridge materials in Figs. 1 and 2. In general, weak localization peaks are easily observable for frequencies within ±5% of ω_T^{ridge}. In the case of ZnS, the results in Fig. 3 are distorted due to the overlapping of the two enhancement peaks.

The above considerations are for interfaces formed from identical ridges. It is interesting to generalize these to treat interfaces of ridges that have a statistical distribution of widths and heights. The weak localization effects in such systems depend on the statistical properties of the width and height distributions characterizing the ridges on the interface.

IV. RESULTS FOR RANDOMLY SHAPED RIDGES

In this section the light scattered from an interface of Gaussian ridges of identical dielectric medium but characterized by random height and width parameters is studied. As in the previous section the axes of the ridges are parallel and are randomly placed with a low ridge covering concentration

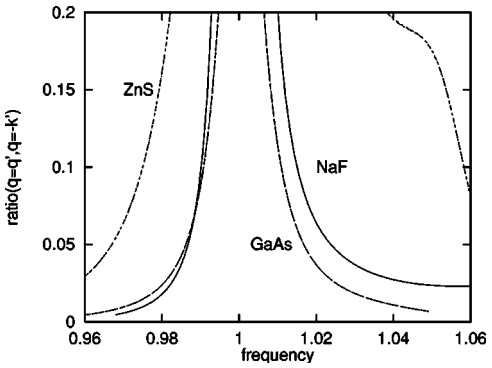

FIG. 3. Plot of the absolute value of the ratio of the first ladder diagram divided into the sum of the contributions of the second ladder and first maximally crossed diagrams for the weak localization peaks versus ω/ω_T^{ridge}. Plots are shown for $\theta_s'=-10°$ (memory effect) and $\theta_s'=-20°$ (time-reversed memory effect) where the results for the memory effect and time-reversed memory effect cannot be distinguished on the scale of the plot. For these plots $\theta_i=20°$ and $\theta_s=-10°$. The results for $\theta_s'=-10°$ and $\theta_s'=-20°$ cannot be distinguished on the scale of the plot. Curves are labeled for the various ridge materials.

on the semi-infinite CdS substrate. The dielectric material of the ridges differs from that of the semi-infinite substrate. The ith ridge on the interface is characterized by A_i and R_i height and width parameters, and the $\{A_i\}$ and $\{R_i\}$ for the ridges along the interface are statistically independent random variables. The leading order effects of each of these types of interface disorder on the speckle correlations are determined.

The averages in Eqs. (17)–(22) for the speckle correlation function now involve the parameters A_i and R_i associated with the individual ridges as well as the positions of the ridges on the interface. As a consequence, the background and weak localization contributions to the speckle correlation functions can be obtained by making some changes in the formulation in Secs. II and III. This is done by changing the irreducible four vertices and the Green's function self-energy in Secs. II and III to take into account the averages over A_i and R_i. The vertex $\Gamma_0(q,r|p,s)$ in Eq. (26) is replaced by

$$\begin{aligned}\Gamma_0(q,r|p,s) &\approx \frac{\pi}{\Delta x}c_{av}v^*(q|r)v(p|s)[\langle A_i^2R_i^2e^{-(q-r)^2R_i^2/2}\rangle_r \\ &\quad - c_{av}\langle A_iR_ie^{-(q-r)^2R_i^2/4}\rangle_r^2] \\ &\approx \frac{\pi}{\Delta x}c_{av}v^*(q|r)v(p|s)\langle A_i^2R_i^2e^{-(q-r)^2R_i^2/2}\rangle_r\end{aligned} \tag{41}$$

where $\langle\ \rangle_r$ denotes an average over the A_i and R_i and $\tilde{\Gamma}_0(q,r|p,s)$ in Eq. (28) is replaced by

$$\begin{aligned}\tilde{\Gamma}_0(q,r|p,s) &\approx \frac{\pi}{\Delta x}c_{av}v(q|r)v(p|s)[\langle A_i^2R_i^2e^{-(q-r)^2R_i^2/2}\rangle_r \\ &\quad - c_{av}\langle A_iR_ie^{-(q-r)^2R_i^2/4}\rangle_r^2] \\ &\approx \frac{\pi}{\Delta x}c_{av}v(q|r)v(p|s)\langle A_i^2R_i^2e^{-(q-r)^2R_i^2/2}\rangle_r.\end{aligned} \tag{42}$$

The Green's function self-energy in Eq. (31), modified for distributed A_i and R_i, is obtained from Eq. (32) taking $V_0(k)=\sqrt{\pi}c_{av}(\langle A_iR_i\rangle_r/\Delta x)v(k|k)$ and using Eq. (42) for $\tilde{\Gamma}_0(p,k|p,k)$. For the plots in this section, the Green's function self-energy corrections due to surface scattering are extremely small and the plasmon-polariton lifetimes are dominated by dielectric losses. As a result, the widths of the weak localization peaks [from Eqs. (36) and (39)], which are set by the Green's function lifetimes, are overwhelmingly determined by the imaginary parts of the dielectric constants. The primary effects of A_i and R_i on the speckle correlation functions then arise from the reducible four vertex functions of Eqs. (19), (20), (25), (27), (28), and (30) with Eqs. (41) and (42).

The statistical average $\langle A_i^2R_i^2e^{-(r-s)^2R_i^2/2}\rangle_r$ is needed to evaluate the irreducible four vertex terms in Eqs. (41) and (42). For A_i and R_i statistically independent variables

$$\langle A_i^2R_i^2e^{-(r-s)^2R_i^2/2}\rangle_r=\langle A_i^2\rangle_r\langle R_i^2e^{-(r-s)^2R_i^2/2}\rangle_r, \tag{43}$$

so that the wave vector dependence enters through the second factor on the right-hand side. The leading order effects of height variations are wave vector independent, contributing a renormalization of the overall scattering intensity of various multiple scattering process while affecting their angular distribution to a lesser extent. For our case, in which the Green's function lifetimes are dominated by the imaginary part of the dielectric constants, Eqs. (29)–(39) and (41)–(43) give a simple dependence of $C^{(1)}(q,k|q',k')$ and $C^{(10)}(q,k|q',k')$ on $\langle A_i^2\rangle_r$. To leading order in the perturbation theory, $C^{(1)}(q,k|q',k')$ and $C^{(10)}(q,k|q',k')$ are proportional to $(\langle A_i^2\rangle_r)^2$ while the higher order weak localization terms in $C^{(1)}(q,k|q',k')$ first enter in order $(\langle A_i^2\rangle_r)^3$. This indicates that increasing $\langle A_i^2\rangle_r$ facilitates the observation of weak localization. For the opposite case (not treated here), in which the Green's function surface scattering self-energy corrections dominate over lifetime effects from the imaginary part of the dielectric constants, the localization effects are of order $(\langle A_i^2\rangle_r)^2$. In this limit adjusting the height statistics has little affect on the observation of weak localization.

The dependence of the bracketed term in Eq. (43) on R_i is more complicated than that on A_i. Averaging $R_i^2e^{-(r-s)^2R_i^2/2}$ over R_i produces a function of $(r-s)^2$ that is not a simple Gaussian. For example, for a mean value $\langle R_i\rangle=R$ a Gaussian distribution of the form $[1/(2\pi)^{1/2}\sigma]\exp[-(R_i-R)^2/2\sigma^2]$ gives

$$\langle R_i^2e^{-q^2R_i^2/2}\rangle_r=\frac{\sigma^2}{(1+\sigma^2q^2)^{3/2}}\left[1+\frac{1}{1+\sigma^2q^2}\frac{R^2}{\sigma^2}\right]\times\exp\left[-\frac{q^2R^2}{2}\frac{1}{1+\sigma^2q^2}\right] \tag{44}$$

while a Poisson distribution of the form $(1/R)\exp(-R_i/R)$ gives

$$\langle R_i^2e^{-q^2R_i^2/2}\rangle_r=\frac{1}{2R|q|^3}\sum_{n=0}^{\infty}\frac{1}{n!}\frac{(-1)^n}{(|q|R)^n}\Gamma\left(\frac{n+3}{2}\right). \tag{45}$$

In the following we will concentrate on the more complex R_i dependence, only briefly mentioning some effects of a distribution of A_i. In the numerical illustrations we will focus on the Gaussian distribution in Eq. (44).

Before discussing the speckle correlation function for a system of ridges of random widths and heights it is necessary to determine the differential reflection coefficient of the surface. The differential reflection coefficient results presented in Ref. 21 were for systems of identical ridges, but can be modified to handle the case of a distribution of ridge widths and heights. This is accomplished by making the same vertex and Green's function replacements as are made in the expressions for the speckle correlation functions. An outline of the required changes is given below. To shorten the presentation below, only an interface of GaAs ridges on the CdS substrate will be studied.

The differential reflection coefficient for the diffuse scattering is given by[12,21]

$$\frac{dR_e}{d\theta_s}(q|k)_{diff}=\frac{2}{\pi}\alpha_0^2(q)\alpha_0(k)|G(q)|^2|G(k)|^2\tau^{(t)}(q|k), \tag{46}$$

where $\tau^{(t)}(q|k)$ is the reducible four vertex function. In the approximation that the reducible four vertex function is from the first two ladder diagrams and the lowest maximally crossed diagram and that the Green's function is obtained using the method discussed below Eqs. (41) and (42):[21]

$$\tau^{(t)}(q|k)=\Gamma_0(q,k|q,k)+\int\frac{ds}{2\pi}\Gamma_0(q,s|q,s)|G(s)|^2\Gamma_0(s,k|s,k)+\int\frac{ds}{2\pi}\Gamma_0(q,q+k-s|s,k)G^*(q+k-s)\times G(s)\Gamma_0(q+k-s,k|q,s). \tag{47}$$

The differential reflection coefficient of the GaAs—CdS interface then follows from Eqs. (41), (42), (46), and (47). For simplicity, in our discussions below, the parameters $A_i=A$ so that $\langle A_i^2\rangle_r=A^2$, and Eq. (44) is used to treat the randomness of R_i. The geometry of the interface for both the differential reflection coefficient results and the subsequent discussions in this section of the speckle correlation function is given by $(\omega_T^{GaAs}/c)A=0.05$, $(\omega_T^{GaAs}/c)\langle R_i\rangle_r=1.0$, and $(\omega_T^{GaAs}/c)\Delta x=0.1$ while $c_{av}=0.001$. Results for the differential reflection coefficient and speckle correlation function near the dielectric resonance frequency are studied as a function of the rms, σ, of the distribution of R_i.

The effects of a statistical distribution of ridge widths and heights on the differential reflection coefficient are computed for $(\omega_T^{GaAs}/c)\sigma$ ranging from 0.0 to 0.5 at a fixed frequency of light that is slightly below the dielectric resonance frequency. In Fig. 4 plots are presented of the differential reflection coefficient of the GaAs—CdS interface as a function of θ_s for $\theta_i=10°$ with $\omega/\omega_T^{GaAs}=0.988$. The curves have been normalized so that the area under each curve for $-90°\leqslant\theta_s\leqslant 90°$ is unity. This facilitates the comparison of

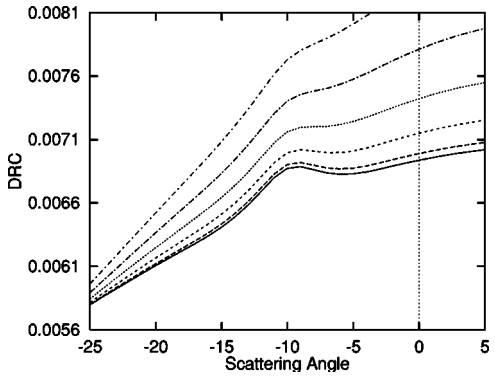

FIG. 4. Plot of the differential reflection coefficient vs scattering angle θ_s for a GaAs—CdS system for *p*-polarized light at $\theta_i=10°$. For this plot $\omega/\omega_T^{GaAs}=0.988$. The curves are (from bottom to top) for $(\omega_T^{GaAs}/c)\sigma=0.0$, 0.1, 0.2, 0.3, 0.4, and 0.5. The area under each curve is normalized to unity over the interval $-90° \leqslant \theta_s' \leqslant 90°$.

the enhancement peaks with the background contributions. As our focus is on the weak localization effects, the scattering angle θ_s has been limited to the interval $-25°$ and $5°$ centered about the $\theta_s=-10°$ localization peak. It is seen from Fig. 4 that increasing σ gradually washes out the backscattering (weak localization) peak. At $(\omega_T^{GaAs}/c)\sigma=0.4$ the enhancement is essentially a shoulder on the diffuse scattering. On the other hand, increasing A, as per our discussions above, accentuates the backscattering peak. The width of the backscattering peak, which is determined primarily by the imaginary part of the dielectric constant of the CdS substrate, is little affected by σ.

The correlation functions for the random interface are obtained from Eqs. (34)–(39) together with (41) and (42). In Fig. 5 $C^{(1)}$ vs θ_s' is presented for the system studied in Fig. 4. Only the $C^{(1)}$ correlations are given as these contain the weak localization effects. In Fig. 5 results for $C^{(1)}$ for $(\omega_T^{GaAs}/c)\sigma$ between 0.0 and 0.5 are shown computed for $\theta_i=20°$ and $\theta_s=-10°$ fixed, allowing θ_s' to run from $-45°$ to $0°$. This region of θ_s' includes the weak localization peaks at $\theta_s'=-10°$ (memory) and $\theta_s'=-20°$ (time-reversed memory). These have the same widths as the weak localization peaks in

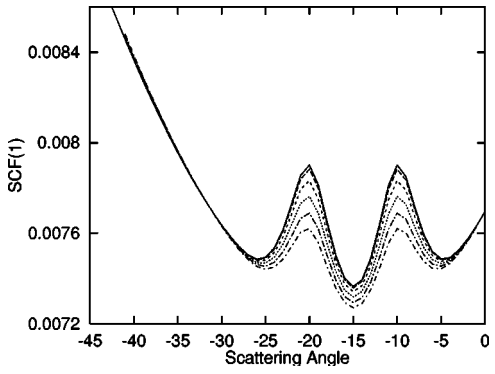

FIG. 5. Plot of $C^{(1)}(q,k|q',k')$ vs θ_s' for $\theta_i=20°$ and $\theta_s=-10°$ for the GaAs—CdS interface. Curves are presented for (from top to bottom) $(\omega_T^{GaAs}/c)/\sigma=0.0$, 0.1, 0.2, 0.3, 0.4, and 0.5. The frequency is $\omega/\omega_T^{GaAs}=0.988$. The area under each curve is normalized to unity over the interval $-90° \leqslant \theta_s' \leqslant 90°$.

the differential reflection coefficients of Fig. 4 and are primarily determined by the imaginary part of the CdS dielectric constant. Increasing σ washes out the phase coherent peaks in the speckle correlation function and increases the peak widths. The variation in the geometric features characterized by the ridge width parameter tends to disrupt the phase coherence in the net scattering from the random interface while increasing A enhances ridge scattering and tends to accentuate the peaks of the phase coherent scattering. The curves in Fig. 5 are all normalized to enclose unit area over the interval $-90° \leqslant \theta_s' \leqslant 90°$. This has been done as we are interested in the relative contrast between the weak localization contributions to the speckle correlation functions with those not related to weak localization. In general, the weak localization effects in both the differential reflection coefficients and speckle correlation functions are relatively stable against statistical variations in the width and height parameters characterizing the ridges on the interface.

V. STUDY OF THE $C^{(1.5)}$, $C^{(2)}$, AND $C^{(3)}$ SURFACE POLARITON EFFECTS

In this section the $C^{(1.5)}(q,k|q',k')$, $C^{(2)}(q,k|q',k')$, and $C^{(3)}(q,k|q',k')$ contributions to the speckle correlation function are briefly presented.[18,19] These occur, respectively, in orders $\zeta^6 L$, $\zeta^8 L$, and $\zeta^{12} L$ of the perturbation expansion, and though they contain peaks as functions of the scattering angle θ_s' these are related to the poles of the surface plasmon-polariton Green's function, not to weak localization effects. The frequency dependence of the peaks near the dielectric resonance frequency of the ridge material is studied and the peak widths are found to be little affected by the resonance. The widths are shown to be increasing functions of frequency through the resonance. A sharp increase in the overall intensity of the $C^{(1.5)}$, $C^{(2)}$, and $C^{(3)}$ terms is found near the resonance frequency. The results for $C^{(1.5)}$, $C^{(2)}$, and $C^{(3)}$ are presented here for completeness, with only the GaAs—CdS interface of identical random ridges treated.

Typical diagrammatic contributions to $C^{(1.5)}$, $C^{(2)}$, and $C^{(3)}$ are shown in Figs. 6. (A complete enumeration of all the diagrams used to compute these various contributions to the speckle correlation functions are given in Figs. 2, 3, and 4 of Ref. 18.) For the results in this paper, the diagrams in Figs. 6 along with those in the more complete enumeration in Ref. 18 are evaluated using the Green's functions and irreducible four vertex functions in Secs. II and III. In this notation the diagram in Fig. 6(a), for example, is interpreted to give the contribution

$$\begin{aligned} C_a^{(1.5)}(q,k|q',k') = LF(q,k|q',k')|G(q)G(k)G \\ \times(q')G(k')|^2|G(k-k'+q')|^2 \times |\Gamma_0(k-k' \\ +q',k|q',k')|^2\Gamma_0(q,k-k'+q'|q,k-k' \\ +q'). \end{aligned} \tag{48}$$

Here L is the length of the surface in the x_1 direction, and the subscript a on the left hand side indicates that $C_a^{(1.5)}$ is one of the terms summed over to give $C^{(1.5)}$. The presence of $|G(k-k'+q')|^2$ in Eq. (48), gives peaks from the Green's function

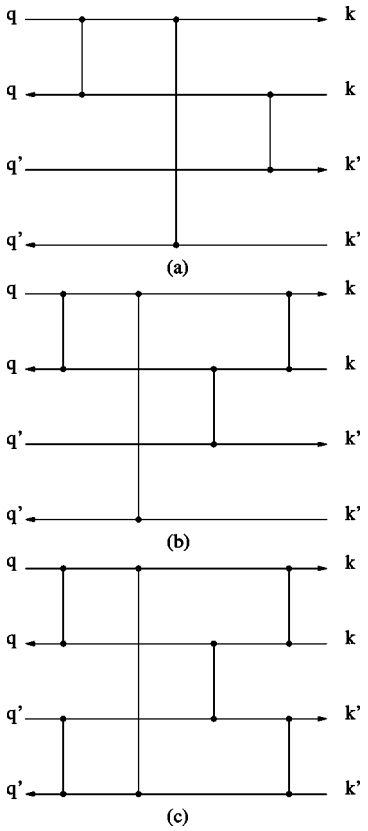

FIG. 6. A typical diagram (see Figs. 2, 3, and 4 of Ref. 18 for a complete enumeration) for (a) $C^{(1.5)}(q,k|q',k')$, (b) $C^{(2)}\times(q,k|q',k')$, and (c) $C^{(3)}(q,k|q',k')$.

poles at $k-k'+q'=\pm K_{sp}$ where K_{sp} is the wavenumber of the surface plasmon-polariton. (Similar pole contributions are associated with the other diagrammatic contributions.[18]) The width of the peaks in $C^{(1.5)}$ follows from the imaginary part of the substrate dielectric constant and from the imaginary part of the self-energy correction to the pole of the single-particle Green's function. The self-energy correction to the Green's function poles is primarily determined by the imaginary part of the GaAs and CdS dielectric constants.

In Figs. 7 results are presented for the $C^{(1.5)}(q,k|q',k')$, $C^{(2)}(q,k|q',k')$, and $C^{(3)}(q,k|q',k')$ contributions to the speckle correlation function for the GaAs—CdS interface studied in Sec. III. The contributions are plotted as functions of θ_s' for fixed $\theta_i=20^\circ$, $\theta_s=-10^\circ$, and $\theta_i'=30^\circ$. [Here the same angles as in Ref. 18 have been taken to facilitate a comparison of our results with those of Ref. 18 for scattering from a different (metal-vacuum) type of interface.] Curves are shown for a number of frequencies approaching the resonant frequency at ω_T^{GaAs} from above and below. Our interest is in the effects of the resonance on the peaked features of $C^{(1.5)}$ and $C^{(2)}$ so that the area below each curve is normalized to unity. This aids in assessing the prominence of the peaked features in each of these contributions to the speckle correlation functions. As the resonance is approached, the scattering of surface plasmon-polaritons at the interface increases, but the effects of this scattering on surface plasmon polaritons is in general smaller than the effects of the dielectric losses that are modeled by the imaginary part of the dielectric constant. The total surface plasmon-polariton losses due to scattering and the imaginary part of the dielectric constant show up as a broadening of the Green's function poles and of the correlation function peaks due to the decrease in the plasmon-polariton lifetime. In general, these effects just increase with increasing frequency through and past the resonance.

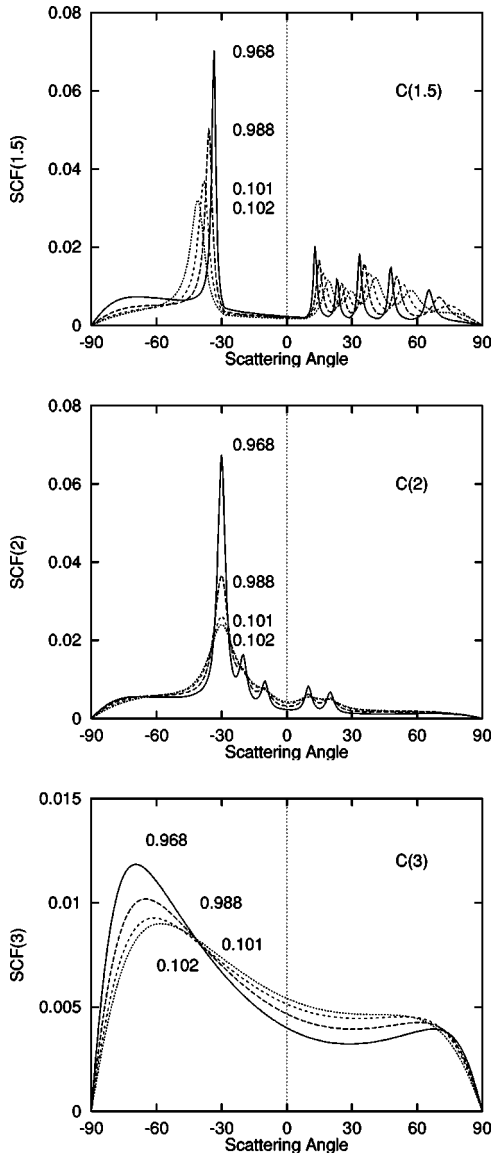

FIG. 7. Plots vs θ_s' of (a) $C^{(1.5)}(q,k|q',k')$, (b) $C^{(2)}\times(q,k|q',k')$, and (c) $C^{(3)}(q,k|q',k')$. Results are shown for GaAs system in Fig. 1 for the frequencies $f=\omega/\omega_T^{GaAs}=0.968$, 0.988, 0.1010, and 0.1020 shown on the figures. (Note: The largest peak in each figure is observed to decrease with increasing frequency.) The plots are normalized to have unit area under each of the curves presented.

As a final note we point out that, for the models treated in this paper, there is a term neglected in the factorization of Eq. (16) that contributes to the correlation functions to order $L\zeta^4$. This term dominates over the $C^{(1.5)}$, $C^{(2)}$, and $C^{(3)}$ terms, but it is continuous and displays no interesting features. It is the singularities in $C^{(1.5)}$ and $C^{(2)}$ that are of interest and of

physical significance in our discussions. Specifically, to leading order, in the absence of the factorization approximation

$$\langle |G(q|k)|^2 |G(q'|k')|^2 \rangle \approx |G(q)G(k)G(q')G(k')|^2 |v(q|k)v(q'|k')|^2 \times \frac{c_{av}}{\Delta x} L\pi^2 A^4 R^4 e^{-[(q-k)^2+(q'-k')^2](R^2/2)}, \quad (49)$$

which contributes of order $\zeta^4 L$ to $C(q,k|q',k')$ through Eq. (15). In the previous sections, we have focused on terms in the speckle correlation function arising from the factorization approximation in Eq. (16) because the factorization approximation leads to a treatment of the properties of $C^{(1)}$ and $C^{(10)}$. These are the dominant terms of the correlations function. Away from the regions over which $C^{(1)}$ and $C^{(10)}$ are nonzero, however, the smoothly varying contributions from Eq. (49) must be included. These contributions, however, do not mask the singularities in the $C^{(1.5)}$ and $C^{(2)}$ terms.

VI. SPECKLE FROM SURFACES THAT ARE PERIODIC ON AVERAGE

An interesting case for the diffuse scattering of light is a random surface that is periodic on average.[32] Consider a periodic array of identical Gaussian ridges that are placed along the x_1 axis of a vacuum-CdS planar interface such that the periodicity of the array has a lattice constant a and there are $N \to \infty$ lattice sites on the surface. The array, then, is described by Eq. (1) with $x_{1j}=ja$. A random surface that is periodic on average can be made by removing, at random along the interface, a fractional concentration of ridges from the lattice. The resulting random systems then has a concentration c_{av} of ridges remaining on the lattice.

The Fourier transform of the configuration average of the random surface profile function along the interface is given by

$$\langle \hat{\zeta}(p) \rangle = c_{av}\sqrt{\pi} A R e^{-p^2R^2/4} \sum_n \frac{2\pi}{a}\delta\left(p - \frac{2\pi}{a}n\right) \quad (50)$$

and the Fourier transforms of the correlation functions of the surface profile function are given by

$$\langle \hat{\zeta}^*(p)\hat{\zeta}(q) \rangle = \pi A^2 R^2 e^{-(p^2+q^2)R^2/4}\left[c_{av}^2 \sum_{n,m} \frac{2\pi}{a}\delta\left(p - \frac{2\pi}{a}n\right)\frac{2\pi}{a}\delta\left(q - \frac{2\pi}{a}m\right) + c_{av}(1 - c_{av})\sum_n \frac{2\pi}{a}\delta\left(p - q - \frac{2\pi}{a}n\right)\right], \quad (51)$$

$$\langle \hat{\zeta}(p)\hat{\zeta}(q) \rangle = \pi A^2 R^2 e^{(p^2+q^2)R^2/4}\left[c_{av}^2 \sum_{n,m} \frac{2\pi}{a}\delta\left(p - \frac{2\pi}{a}n\right)\frac{2\pi}{a}\delta\left(q - \frac{2\pi}{a}m\right) + c_{av}(1 - c_{av})\sum_n \frac{2\pi}{a}\delta\left(p + q - \frac{2\pi}{a}n\right)\right]. \quad (52)$$

If Eqs. (50)–(52) are used in the discussions given in Sec. II and III, results are obtained for the differential reflection coefficient and speckle correlation function of the diffuse scattering from a random surface that is periodic on average. The presence of a randomness that is periodic on average gives rise to enhancement peaks in the differential reflection coefficient that are found when $q+k+(2\pi/a)n \approx 0$ for n an integer. (Remember: For the random interface without an average periodicity the differential reflection coefficient exhibits only the $n=0$, $q+k=0$, weak localization peak.) For the speckle correlation functions of the periodic on average system $C^{(1)}(q,k|q',k') = (2\pi/a)\Sigma_n \delta[q-k-q'+k'-(2\pi/a)n] \times C_n^{(1)}(q,k|q',k')$ where $C_n^{(1)}(q,k|q',k')$ is an envelop function and $C^{(10)}(q,k|q',k') = (2\pi/a)\Sigma_n \delta[q-k+q'-k' -(2\pi/a)n] C_n^{(10)}(q,k|q',k')$ where $C_n^{(10)}(q,k|q',k')$ is an envelop function. Not only are the number of envelop functions increased in $C^{(1)}$ and $C^{(10)}$, but, as we shall see below, additional phase coherent peaks are found in the envelop functions of $C^{(1)}$. In the absence of an average periodicity only the $n=0$ terms $C_0^{(1)}$ and $C_0^{(10)}$ survive and the results in Secs. II and III are obtained. In the following we shall limit our discussions to the $n=0$ terms in the $C^{(1)}$ series for the periodic on average surface. (A discussion of the other terms will be presented elsewhere.)

Again, for the periodic on average system, the $C^{(1)} \times (q,k|q',k')$ term in the correlation function contains phase coherent effects associated with weak localization. Considering the $C_0^{(1)}(q,k|q',k')$ envelop function of the periodic on average system: We find that in the perturbation approximation of this paper the reducible four vertex for this envelop function is expressed as the sum of three terms. The first is from the single runged ladder diagram

$$2\pi\delta(q-k-q'+k')\Gamma_{p,0}(q,k|q',k'). \quad (53)$$

Here the lowest order four-vertex envelop function of the periodic on average system for $n=0$ is given by

$$\Gamma_{p,0}(q,k|q',k') = \pi\frac{c_{av}(1-c_{av})}{a} v^*(q|k)v(q'|k') \times A^2R^2 e^{-[(q-k)^2+(q'-k')^2]R^2/4}. \quad (54)$$

The second is from the double runged ladder diagram given by

$$2\pi\delta(q-k-q'+k')\sum_m \int \frac{du}{2\pi}\Gamma_{p,0}\left(q,q-q'+u - \frac{2\pi}{a}m|q',u\right) \quad (55)$$

$$G^*\left(q-q'+u-\frac{2\pi}{a}m\right)G(u)\Gamma_{p,0}\left(q-q'+u-\frac{2\pi}{a}m,k|u,k'\right)$$

and the third (from the lowest order maximally crossed diagram) term is given by

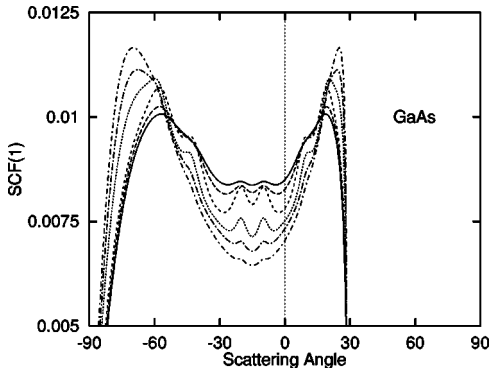

FIG. 8. Plot of $C_0^{(1)}(q,k|q',k')$ of a periodic on average random system vs θ_s' for $\theta_i=20°$ and $\theta_s=-10°$ for a GaAs—CdS interface. Results are shown for $\omega/\omega_T^{GaAs}=1.020$, 1.016, 1.010, 0.988, 0.980, 0.972 (top to bottom at the $\theta_s'=-20°$ localization peak). All curves have been normalized to have unit area under the curve. The resonance frequency is $\omega/\omega_T^{GaAs}=1$.

$$2\pi\delta(q-k-q'+k')\sum_m \int \frac{du}{2\pi}\Gamma_{p,0}\left(q,q+k'-u-\frac{2\pi}{a}m|u,k'\right)$$

$$G^*\left(q+k'-u-\frac{2\pi}{a}m\right)G(u)\Gamma_{p,0}\left(q+k'-u-\frac{2\pi}{a}m,k|q',u\right). \tag{56}$$

Replacing $\hat{L}(q,k|q',k')$ in Eq. (39) by the sum of Eqs. (53), (55), and (56) and substituting into Eq. (34) gives the $C_0^{(1)}\times(q,k|q',k')$ envelop function for the periodic on average surface.

In Fig. 8 results for $C_0^{(1)}(q,k|q',k')$ vs θ_s' for $\theta_i=20°$ and $\theta_s=-10°$ are shown for the case of GaAs ridges on a CdS substrate. For the plots we have taken $(\omega_T^{ridge}/c)A=0.05$, $(\omega_T^{ridge}/c)R=1.0$, $(\omega_T^{ridge}/c)a=4\pi$, and $c_{av}=0.04\pi$ (c_{av} is the average ridge concentration on the periodic interface sites). Results are shown for a number of frequencies in the neighborhood of the dielectric resonance of the ridge material. It is interesting to note that, in addition to the $m=0$ peaks at $\theta_s'=-10°$ ($q'=q$ memory effect) and $\theta_s'=-20°$ ($q'=-k$ time reversed memory effect), peaks from $m=1$ and $m=-1$ are found at $\theta_s'\approx 19.0°$ ($m=-1$ memory effect), $\theta_s'\approx -42.3°$ ($m=1$ memory effect), $\theta_s'\approx 9.1°$ ($m=1$ time-reversed memory effect), and $\theta_s'\approx -57.4°$ ($m=-1$ time-reversed memory effect). The additional peaks (i.e., the peaks with $m\neq 0$) arise from phase coherent scattering processes that involve an intermediary Bragg reflection. Most of the additional peaks are seen in Fig. 8, but some are masked by the shoulders near $\theta_s'=-65°$ and 25° in the single runged ladder contribution to the diffuse scattering. All of the phase coherent peaks are found to be enhanced near the dielectric resonance of the ridge material.

VII. CONCLUSIONS

The effects of resonant dielectric material on weak localization contributions to the speckle correlation function for a random interface were determined. The scattering at the surface is found to exhibit increased weak localization effects near the dielectric resonance frequency of surface media for $C^{(1)}$ contributions to the speckle correlation function. The enhancement of weak localization effects arises from the increased coupling of bulk modes to surface modes and to the increase of multiple scattering of surface modes on the scattering interface. Increasing the disorder on the random interface by allowing the ridges of resonant dielectric material to have statistically distributed widths was shown to decrease weak localization effects in the surface scattering. Peaks in the higher order $C^{(1.5)}$ and $C^{(2)}$ contributions to the speckle correlation function were found to be less affected by resonant dielectric features, the primary effect being peak width broadening due to the decrease in surface plasmon-polariton lifetimes. The origin of these features are not dominated by phase coherent multiple scattering processes to the extent that the origin of weak localization features are but are dominated by dielectric losses. They are less sensitive to the enhancement of multiple scattering. Treatment was also given of random surfaces that are periodic on average. These surfaces exhibit additional weak localization peaks in their correlation functions arising from Bragg reflections. Enhancement of weak localization from surfaces with dielectric resonances was also found for the periodic on average systems.

As a final point we note that the weak localization enhancement effects in both the scattering cross sections and the speckle correlation functions are essentially phase coherent effects. The resonance in the dielectric materials is only used to accentuate these phase coherent effects. Far from the resonance frequency weak localization enhancements are still present in the systems, but they are very small. Phase coherent effects of the type associated with weak localization have a history that precedes their association with weak localization. Early in the study of multiple scattering in disordered media, scattering processes now identified with both ladder and maximally crossed diagrams were used to treat diffuse scattering and backscattering enhancements from random suspensions of particulates.[6,8] The effects now associated with maximally crossed diagrams also show up in the study of double passage effects.[6,8,33] The later association of maximally crossed diagrams with weak localization and strong localization effects was made by Gor'kov *et al.*[34] and Vollhardt and Wolfle[35] in the late 1970s and early 1980s. See also Refs. 6, 8, and 36 in this regard.

[1] A. Ishimaru, *Wave Propagation and Scattering in Random Media* (Academic Press, New York, 1978).
[2] J. A. Ogilvy, *Theory of Wave Scattering from Random Rough Surfaces* (A. Hilger, Philadelphia, 1991).
[3] *Wave Propagation in Random Media*, edited by V. I. Tatarskii, A. Ishimaru, and V. U. Zvorolny (Institute of Physics Publishing, Philadelpha, 1993).
[4] A. A. Maradudin, in *Surface Polaritons*, edited by V. M. Agranovich and D. L. Mills (North-Holland, Amsterdam, 1982).
[5] A. R. McGurn, in *Survey of Semiconductor Physics*, edited by Karl W. Boer (Wiley, New York, 2002).
[6] A. R. McGurn, Surf. Sci. Rep. **10**, 357 (1990).
[7] A. A. Maradudin, T. Michel, A. R. McGurn, and E. R. Mendez, Ann. Phys. **203**, 255 (1990).
[8] A. R. McGurn, Recent Res. Dev. Phys. **3**, 119 (2002).
[9] G. C. Brown, V. Celli, M. Coopersmith, and M. Haller, Surf. Sci. **129**, 507 (1983).
[10] G. C. Brown, V. Celli, M. Haller, A. A. Maradudin, and A. Marvin, Phys. Rev. B **31**, 4993 (1985).
[11] A. A. Maradudin and W. M. Visscher, Z. Phys. B: Condens. Matter **60**, 215 (1985).
[12] A. R. McGurn, A. A. Maradudin, and V. Celli, Phys. Rev. B **31**, 4866 (1985).
[13] A. R. McGurn and A. A. Maradudin, J. Opt. Soc. Am. B **4**, 910 (1987).
[14] *Scattering and Localization of Classical Waves in Random Media*, edited by P. Sheng (World Scientific, Singapore, 1990).
[15] A. R. McGurn and A. A. Maradudin, Phys. Rev. B **39**, 13 160 (1989).
[16] A. Arsenieva and S. Feng, Phys. Rev. B **47**, 13 047 (1993).
[17] M. Nieto-Vesperinas and J. A. Sanchez-Gil, J. Opt. Soc. Am. A **10**, 150 (1993).
[18] V. Malyshkin, A. R. McGurn, T. A. Leskova, A. A. Maradudin, and M. Nieto-Vesperinas, Waves Random Media **7**, 479 (1997).
[19] V. Malyshkin, A. R. McGurn, T. A. Leskova, A. A. Maradudin, and M. Nieto-Vesperinas, Opt. Lett. **22**, 946 (1997).
[20] B. Shapiro, Phys. Rev. Lett. **57**, 2168 (1986).
[21] A. R. McGurn and R. M. Fitzgerald, Phys. Rev. B **65**, 155414 (2002).
[22] D. Sornette and B. Souillard, Europhys. Lett. **7**, 269 (1988).
[23] A. Lagendijk and B. A. van Tiggelen, Phys. Rep. **270**, 143 (1996).
[24] D. A. Wiersma, P. Bartolini, A. Lagendijk, and R. Righini, Nature (London) **390**, 671 (1997).
[25] N. F. Mott and E. A. Davies, *Electronic Processes in Non-Crystalline Solids* (Clarendon Press, Oxford, 1971).
[26] S. Feng, C. Kane, P. A. Lee, and A. D. Stone, Phys. Rev. Lett. **61**, 834 (1988).
[27] R. Berkovits, M. Kaveh, and S. Feng, Phys. Rev. B **40**, 737 (1989).
[28] R. Berkovits and M. Kaveh, Phys. Rev. B **41**, 2635 (1990).
[29] R. Berkovits and M. Kaveh, Europhys. Lett. **13**, 97 (1990).
[30] L. Wang and S. Feng, Phys. Rev. B **40**, 8284 (1989).
[31] R. Berkovits, Phys. Rev. B **42**, 10 750 (1990).
[32] A. A. Arsenieva, A. A. Maradudin, J. Q. Lu, and A. R. McGurn, Opt. Lett. **18**, 1588 (1993).
[33] A. Dogariu, G. D. Boreman, and M. Dogariu, Opt. Lett. **20**, 1665 (1995).
[34] L. P. Gor'kov, A. I. Larkin, and D. E. Khmel'nilskii, Pis'ma Zh. Eksp. Teor. Fiz. **30**, 248 (1979). [JETP Lett. **30**, 228 (1979).]
[35] D. Vollhardt and P. Wolfle, Phys. Rev. B **22**, 4666 (1980).
[36] P. W. Anderson, Physica B & C **117**, 30 (1983).